Acta Materialia 151 (2018) 395–405

Contents lists available at ScienceDirect

Acta Materialia

journal homepage: www.elsevier.com/locate/actamat

Superior twin stability and radiation resistance of nanotwinned Ag solid solution alloy

Jin Li [a], D.Y. Xie [b], S. Xue [a], C. Fan [a], Y. Chen [c], H. Wang [a, d], J. Wang [b, e], X. Zhang [a, *]

[a] School of Materials Engineering, Purdue University, West Lafayette, IN, 47907, USA
[b] Mechanical and Materials Engineering, University of Nebraska-Lincoln, Lincoln, NE, 68583-0857, USA
[c] Department of Chemical Engineering and Materials Science, University of Minnesota, Minneapolis, MN 55455-0132, USA
[d] School of Electrical and Computer Engineering, Purdue University, West Lafayette, IN 47907, USA
[e] Nebraska Center for Materials and Nanoscience, University of Nebraska-Lincoln, Lincoln, NE 68583-0857, USA

ARTICLE INFO

Article history:
Received 5 December 2017
Received in revised form
22 February 2018
Accepted 26 March 2018
Available online 2 April 2018

Keywords:
In situ irradiation
Nanotwinned metal
Twin boundary stability
Solute-twin boundary network

ABSTRACT

Face-centered cubic (FCC) metals are in general vulnerable to high-energy ion irradiation. Twin boundaries have been shown to improve the irradiation tolerance of FCC metals. However, nanotwins in monolithic metals are unstable during irradiation. In this study, we show that Fe solute can drastically improve irradiation stability of twin boundaries in Ag. By adding merely 1 at.% of Fe solute atoms into Ag matrix, ultra-high-density twins with an average twin thickness of ~3 nm form in Ag. *In situ* Kr ion irradiation studies show that defect size and density in $Ag_{99}Fe_1$ have been significantly reduced comparing with monolithic coarse-grained Ag and nanotwinned Ag. Furthermore, these extremely fine twins survived heavy ion irradiations. Density function theory calculations suggest that Fe solutes stabilize nanotwins by pinning twin boundaries. The mechanisms of enhanced radiation tolerance enabled by solute-twin boundary networks are discussed.

1. Introduction

Irradiation of metallic materials by energetic particles, such as neutrons and heavy ions, introduces a large population of point defects and larger defect clusters, such as dislocation networks, stacking fault tetrahedrons (SFTs) and voids. Such significant microstructure damage can degrade mechanical properties [1–5] and thermal and electrical conductivity [1,2], and lead to dimensional changes, such as swelling [1,3–8]. The irradiation tolerance of a material can be enhanced through introducing defect sinks, such as grain boundaries (GBs) [9–14], twin boundaries (TBs) [15–19], free surfaces [20–24,95], and phase boundaries [25–29], which facilitate the recombination of irradiation-induced defects and defect clusters.

GBs are defect sinks to absorb and eliminate irradiation-induced defects [11,13,30–32]. Prior studies show the grain-size effect on the alleviation of irradiation-induced defects in neutron-irradiated alloys [2,33,34]. Sun et al. showed, via *in situ* Kr ion irradiation, that high angle GBs in nanocrystalline Ni can capture interstitial loops and dislocation segments [35]. Molecular dynamics simulations showed that GBs can also emit interstitials into the grain interior to annihilate irradiation-induced vacancies [31]. Furthermore, there are increasing experimental evidence showing that nanocrystalline metals contain lower helium bubble density than their coarse-grained counterparts irradiated to the same doses [11,36].

Coherent twin boundaries (CTBs) are a special type of GBs without apparent free volume and are normally considered to be ineffective defect sinks [12,37]. Han et al. showed that the width of He bubble denuded zones in non-Σ3 GBs is much greater than that in Σ3 CTBs, indicating CTBs have low efficiency in eliminating defects [12]. However, several recent studies have shown that CTBs can remove irradiation-induced defects, such as SFTs in face-centered cubic (FCC) metals, and interstitial clusters [15,17,18,38,39]. Recent studies have also shown that the interactions of CTBs with defects induce steps and stacking faults [40–42]. These steps provide fast-diffusion channels to promote point defect migration and annihilation mainly due to the confinement of migration from 3D to 1D along dislocations. Similar to grain boundary affected zones (or grain boundary denuded zones), where dislocation loops or He bubbles exhibit significantly lower concentration near GBs [12,43–45], twin boundary affected zones have been observed in nanotwinned (NT) Ag, as evidenced by

* Corresponding author.
E-mail address: xzhang98@purdue.edu (X. Zhang).

https://doi.org/10.1016/j.actamat.2018.03.052
1359-6454/

twin-thickness dependent accumulation of irradiation-induced defects [17,46].

Although TBs can improve radiation resistance of metallic materials, radiation-induced detwinning occurs during radiation of monolithic metals. For instance *in situ* Kr ion radiation has shown the migration of TBs in NT Cu [39,47] and NT Ag [48], and the migration velocity of TBs depends on twin thickness [39,47]. To enhance the radiation resistance of metallic materials via twin boundaries, it is necessary to improve the radiation stability of TBs.

Numerous studies have shown that a small amount of solute atoms can significantly amend irradiation-induced microstructures in metallic materials [49–53]. For instance, it has been shown that neutron irradiation-induced interstitials in Al can be trapped by Co substitutional atoms [54]. Detrapping occurs when vacancies become mobile and migrate to the trapped interstitials. Solute atoms may also decrease the diffusion rate of interstitial clusters, and therefore, increase the recombination rate of those clusters with freely migrating vacancies [55]. The influence of solute atoms on irradiation stability of NT metals, however, has not been investigated to date.

The usage of defect sink networks may improve radiation tolerance of metallic materials [56]. For instance, FCC metals such as Ag and Cu are vulnerable to irradiation [38,57–63]. Introduction of high-density defect sink networks, such as TBs and nanopores, has been demonstrated to enhance the irradiation tolerance of nanostructured Ag and Cu [15,17,18,42]. Here we show that solute-TB networks can enable outstanding radiation resistance of FCC metals. Based on a series of *in situ* studies, we discovered that the addition of a small amount of Fe solutes, merely 1 at.%, in Ag can lead to the formation of ultra-high-density twins (~3 nm-thick) with significantly improved irradiation stability. Both the size and density of irradiation-induced defect clusters in Ag-1 at.%Fe solid solution alloys (referred to as $Ag_{99}Fe_1$ hereafter) have been significantly reduced comparing with monolithic coarse-grained Ag and nanotwinned Ag. Density function theory (DFT) calculations suggest that substitutional Fe solutes stabilize nanotwins by pinning incoherent twin boundaries (ITBs) and effectively promote the point defect recombination. The outstanding stability of solute-TB networks has important implication for the design of NT alloys for extreme radiation environment.

2. Experimental

Ag and $Ag_{99}Fe_1$ (in atomic percent) thin films with thickness of 1 μm were deposited onto HF etched Si (111) substrates and SiO_2 substrate via DC magnetron sputtering at room temperature. The targets are pure Ag (99.99%) and Fe (99.95%). A base pressure of ~5×10^{-8} torr was achieved before deposition, and the Ar pressure during deposition was ~2 mtorr.

In situ irradiation experiment was performed at room temperature at the IVEM-TANDEM facility at Argonne National Laboratory. 1 MeV Kr^{++} ion beam was used for radiation experiments. The Stopping and Range of Ions in Matter (SRIM) (Kinchin-Pease method) simulation was used to estimate the displacement damage profile (in the unit of displacements-per-atom (dpa)) and Kr ion distribution. Most Kr ions (99.99%) penetrated directly through the TEM specimens and the residual Kr ion concentration in the TEM thin foil is ~0.01 at.%. A maximum fluence of 3×10^{14} ions cm^{-2} corresponding to ~ 1.5 dpa was applied at a dose rate of 2.5×10^{-3} dpa/s. More details can be found in Ref. [17]. During *in situ* Kr ion irradiation, the temperature rise of specimens was less than 10 °C.

X-ray diffraction (XRD) experiments were performed on a PANalytical Empyrean system (Cu Kα radiation) at room temperature. Both cross-sectional and plan-view transmission electron microscopy (TEM) specimens were prepared by grinding, polishing and ion milling by a Gatan PIPS II system. CG Ag samples were obtained from small pieces of Ag target using the same TEM specimen preparation method. All TEM specimens were examined by using a Thermo Fischer Scientific/FEI Talos 200× microscope with Super-X EDS detectors before and after irradiation.

DFT spin polarized calculations were performed by Vienna ab-initio simulation package (VASP) with projector augmented wave (PAW) method [64]. Geometry optimization and energy calculations were carried out with generalized gradient approximation (GGA) approach. During this process, Perdew-Burke-Ernzerhof (PBE) exchange-correlation density function was employed [65,66]. The pseudopotential used in the calculations was generated with electron configuration $4d^{10}5s^1$ and $3d^74s^1$ for Ag and Fe respectively [67]. The kinetic energy cut-off for the plane wave basis set is 400eV. The first Brillouin zone is integrated by K points selected using the Monkhorst–Pack scheme [68]. A $3 \times 3 \times 3$ and a $4 \times 4 \times 1$ M-P k-point grid was used for bulk model and twined model, respectively. The convergence criteria of self-consistent calculations are that the change of total energy is smaller than 10^{-5} eV and the forces acting on the atoms are less than 0.05 eV/Å. For BCC Fe, the optimized lattice is 0.2828 nm and the cohesive energy is 4.855 eV; For FCC Ag, the optimized lattice is 0.4137 nm and the cohesive energy is 2.509 eV.

3. Results

The X-Ray diffraction (XRD) profile in Fig. 1a shows highly {111} textured Ag and $Ag_{99}Fe_1$ films grown on Si (111) substrates. In comparison, $Ag_{99}Fe_1$ on SiO_2 substrates shows polycrystalline nature with (111) texture and a weak Ag (311) peak. The plan-view TEM micrographs in Fig. 1c–e shows that the Ag and $Ag_{99}Fe_1$ films on Si (111) substrates have distinctive grain boundaries. The inserted selected area diffraction (SAD) patterns examined along Ag <111> zone axis indicate the typical single-crystal-like diffraction patterns. However, the diffraction pattern of $Ag_{99}Fe_1$ films on SiO_2 substrate shows a strong (111) and weak (311) diffraction ring, indicating the formation of polycrystalline films. Cross-section TEM (XTEM) micrographs in Fig. 1f–h shows the formation of high-density twin boundaries (TBs) in all films. Based on these observations, we designate NT Ag and S-NT $Ag_{99}Fe_1$ for single-crystal-like nanotwinned Ag, and $Ag_{99}Fe_1$ films, and refer to polycrystalline $Ag_{99}Fe_1$ as P-NT $Ag_{99}Fe_1$ hereafter. The average columnar grain size is 110 ± 20 nm for NT Ag, 110 ± 30 nm for S-NT $Ag_{99}Fe_1$, and 110 ± 30 nm for P-NT $Ag_{99}Fe_1$. The average twin spacing is 13 ± 7, 3 ± 2 and 3 ± 2 nm for NT Ag, S-NT $Ag_{99}Fe_1$ and P-NT $Ag_{99}Fe_1$, respectively. TBs are parallel to the substrate surfaces in the NT Ag and S-NT $Ag_{99}Fe_1$ films, whereas misaligned TBs (with neighboring grains) are observed in P-NT $Ag_{99}Fe_1$. The columnar boundaries in NT Ag and S-NT $Ag_{99}Fe_1$ films are primarily ITBs, and two types of ITBs have been identified: sharp ITBs aligned along the same line (blue arrows in Fig. 1g, and white arrows in Fig. 1f), and diffuse ITBs (yellow arrows in Fig. 1g). P-NT $Ag_{99}Fe_1$ (Fig. 1h) also contains high-angle grain boundaries (between (111) and (311) columnar grains) in addition to ITBs (between adjacent (111) columnar grains).

A summary of irradiation experiments reported in this study is shown in Fig. 1b. Four types of specimens have been studied, including coarse-grained (CG) Ag, NT Ag, S-NT $Ag_{99}Fe_1$ and P-NT $Ag_{99}Fe_1$. All specimens have been irradiated from their plan-view direction. NT-Ag and S-NT $Ag_{99}Fe_1$ have also been irradiated from cross-section direction. High-resolution TEM (HRTEM) images in Fig. 2 show that the CTBs in S-NT $Ag_{99}Fe_1$ are decorated with stacking faults (SFs). The distributions of Ag and Fe in S-NT $Ag_{99}Fe_1$ and P-NT $Ag_{99}Fe_1$ before and after irradiation are shown in EDS composition maps in Suppl. Fig. 1 and Suppl. Fig. 2.

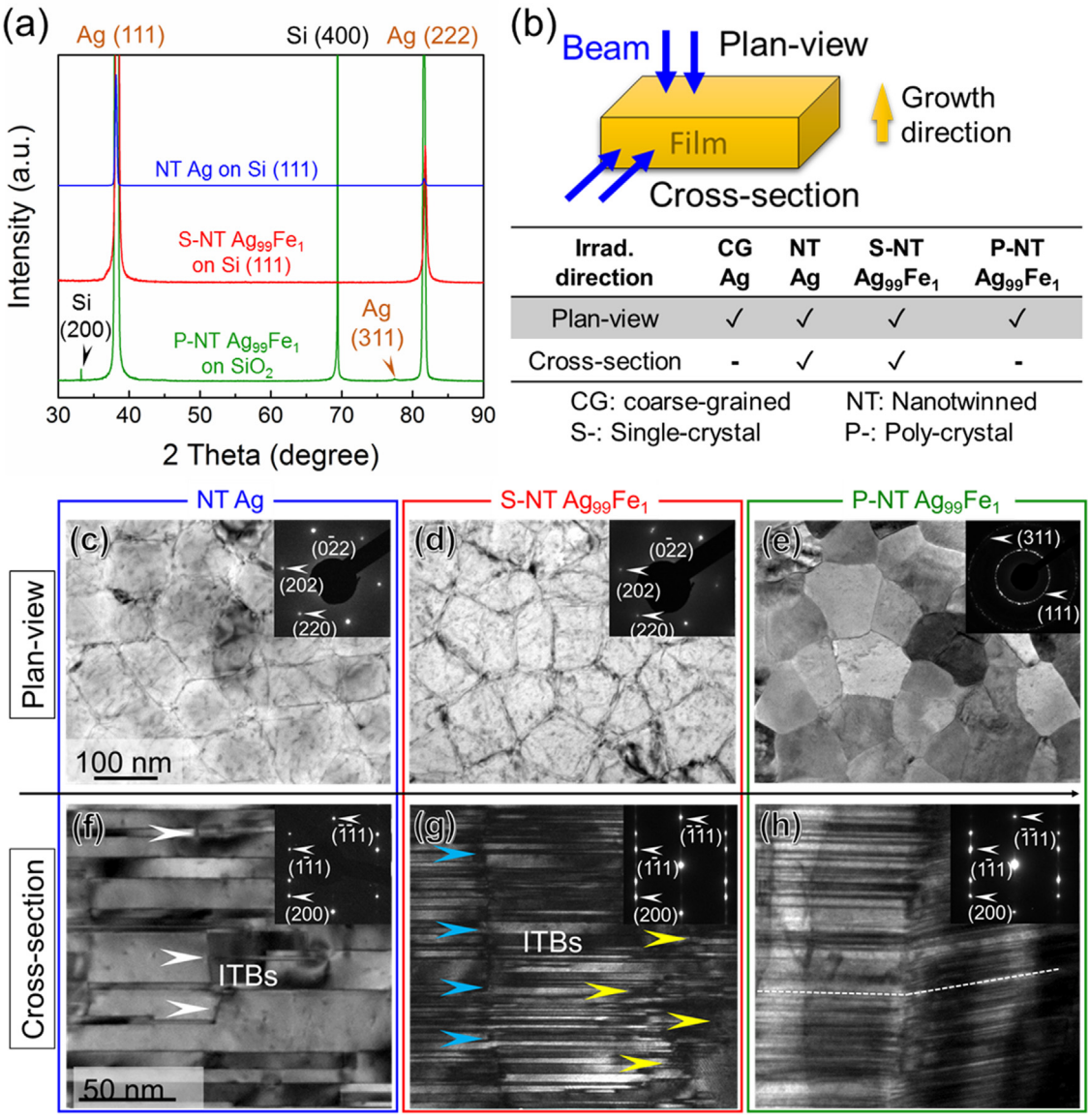

Fig. 1. (a) XRD profile shows highly {111} textured nanotwinned (NT) Ag and S-NT $Ag_{99}Fe_1$ on Si (111) substrate, and P-NT $Ag_{99}Fe_1$ on SiO_2 substrate. (b) Summary of irradiation experiments reported in this study. (c–e) Plan-view TEM images showing grain boundaries in the NT Ag, S-NT $Ag_{99}Fe_1$ and P-NT $Ag_{99}Fe_1$ films. The inserted selected area diffraction (SAD) patterns examined along Ag <111> zone axis exhibit single-crystal-like patterns in NT Ag and S-NT $Ag_{99}Fe_1$, and (111) and a weak (311) diffraction rings in P-NT $Ag_{99}Fe_1$. (f–h) Cross-section TEM (XTEM) micrographs showing the formation of high-density twin boundaries (TBs) in all films. The SAD patterns indicate the formation of classical twinned structures (The SAD pattern in (h) is taken from one of the columnar grains).

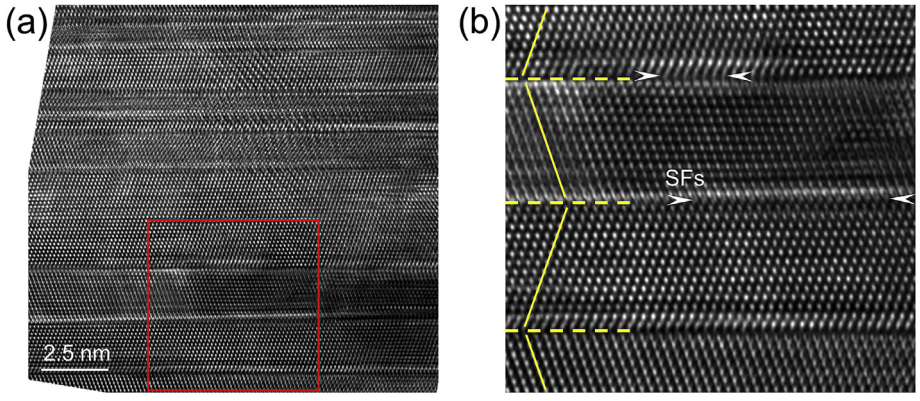

Fig. 2. (a) High-resolution TEM images showing the microstructure of fine twins in S-NT $Ag_{99}Fe_1$. (b) The magnified view of the box in (a) shows (111) CTBs decorated with SFs.

During irradiation, all films accumulate damages, but to a different level. *In situ* video snapshots compare the microstructures of plan-view specimens irradiated to the same dose levels. The CG Ag film accumulated a large number of defect clusters after merely 0.025 dpa, and was significantly damaged by 0.2 dpa as evidenced by dark contrast due to significant overlap of defect clusters (Fig. 3a–c). In irradiated NT Ag, a moderate number of defects were generated, and the grain boundaries are barely discernable by 0.025 dpa. By 0.2 dpa, defect density increases further, and the grain boundaries are invisible (Fig. 3d–f). In the irradiated S-NT $Ag_{99}Fe_1$, fewer defects were generated at 0.025 dpa compared to NT Ag, and most of the grain boundaries are still visible (Fig. 3h). The grain boundaries became indistinguishable at a dose of 0.2 dpa (Fig. 3i). However, the film appears to have smaller and fewer defects compared to NT Ag. Similar to S-NT $Ag_{99}Fe_1$, the P-NT $Ag_{99}Fe_1$ film experiences moderate damage, but some of the grain boundaries in P-NT $Ag_{99}Fe_1$ remain visible after 0.2 dpa (Fig. 3j–l). It is worth mentioning that given the polycrystalline nature of P-NT $Ag_{99}Fe_1$, not all grains appear to contain the similar number of irradiation-induced defects due to imaging conditions. Thus extensive post radiation defect analysis for P-NT $Ag_{99}Fe_1$ was performed by carefully examining grains oriented to the correct imaging conditions.

The XTEM images of NT Ag and S-NT $Ag_{99}Fe_1$ before and after irradiation to 1.5 dpa are compared in Fig. 4. Both specimens have well defined TBs before irradiation (Figs. 4a and 4c). After irradiation to 1.5 dpa, numerous TBs in NT Ag disappeared, and the average twin spacing increased from 13 ± 7 to 22 ± 15 nm. Additionally, most ITBs at the original columnar boundaries are no longer visible after radiation (Fig. 4b). In comparison, the TBs in irradiated S-NT $Ag_{99}Fe_1$ are much more stable (Fig. 4d). After irradiation to 1.5 dpa, few TBs were removed and the average twin spacing increased slightly from 3 ± 2 to 5 ± 3 nm. The sharp ITBs became diffused and less distinguishable after irradiation. Also, the CTBs were decorated with SFs.

The evolution of defect density as a function of irradiation dose is different among four types of specimens. As shown in Fig. 5, the defect density in CG Ag reaches saturation, ~$21.5 \times 10^{22}/m^3$, at ~0.05 dpa, while defect densities in NT Ag, S-NT $Ag_{99}Fe_1$and P-NT $Ag_{99}Fe_1$ gradually increase until 0.2 dpa, and level off at ~10.8, 5.1 and $4.9 \times 10^{22}/m^3$, respectively. Note that defect density analysis reflects a lower bound estimation since not all defects can be resolved during *in situ* TEM studies.

A summary of average grain size, twin spacing (before and after irradiation), defect size and density in all irradiated specimens are given in Table 1. CG Ag has the largest average defect size, ~12 nm. NT Ag has a much smaller average defect size, ~7 nm, followed by 5 nm in both types of $Ag_{99}Fe_1$ specimens. In addition, the average defect size in NT $Ag_{99}Fe_1$ is comparable to their average twin spacing.

4. Discussion

4.1. Energetics of Fe solutes in Ag

NT Ag exhibits enhanced irradiation tolerance compared to CG Ag due to high-density TBs [15,17]. By adding merely ~1 at.% Fe

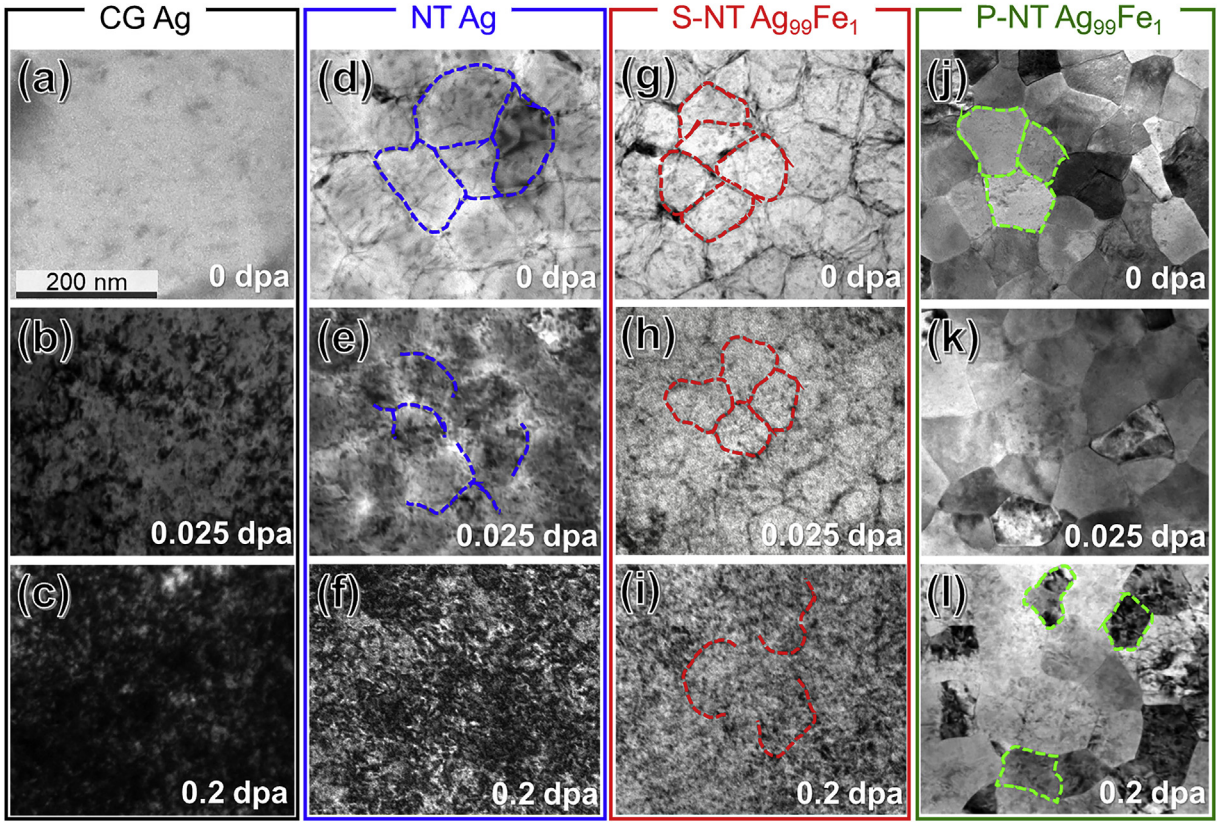

Fig. 3. *In situ* video snapshots recorded during Kr ion irradiation at room temperature compare the irradiation response among all specimens at the same dose levels. The scale bar in (a) applies to all images. (a–c) CG Ag accumulated a large number of defects after 0.025 dpa, and was significantly damaged by 0.2 dpa. (d–f) In irradiated NT Ag, a moderate number of defects are generated within the grains, and the columnar boundaries became blurry by 0.025 dpa. At 0.2 dpa, defect density appeared to increase further, and the columnar boundaries became invisible. (g–i) In S-NT $Ag_{99}Fe_1$, fewer defects were generated at 0.025 dpa compared to NT Ag, and most of the columnar boundaries were still clear at this dose level. The columnar boundaries became indistinguishable at 0.2 dpa. However, the film appeared to have smaller and fewer defects compared to NT Ag. (j–l) Similar to S-NT $Ag_{99}Fe_1$, the P-NT $Ag_{99}Fe_1$ film experienced moderate damage, but some of the grain boundaries in P-NT $Ag_{99}Fe_1$ remained visible after 0.2 dpa.

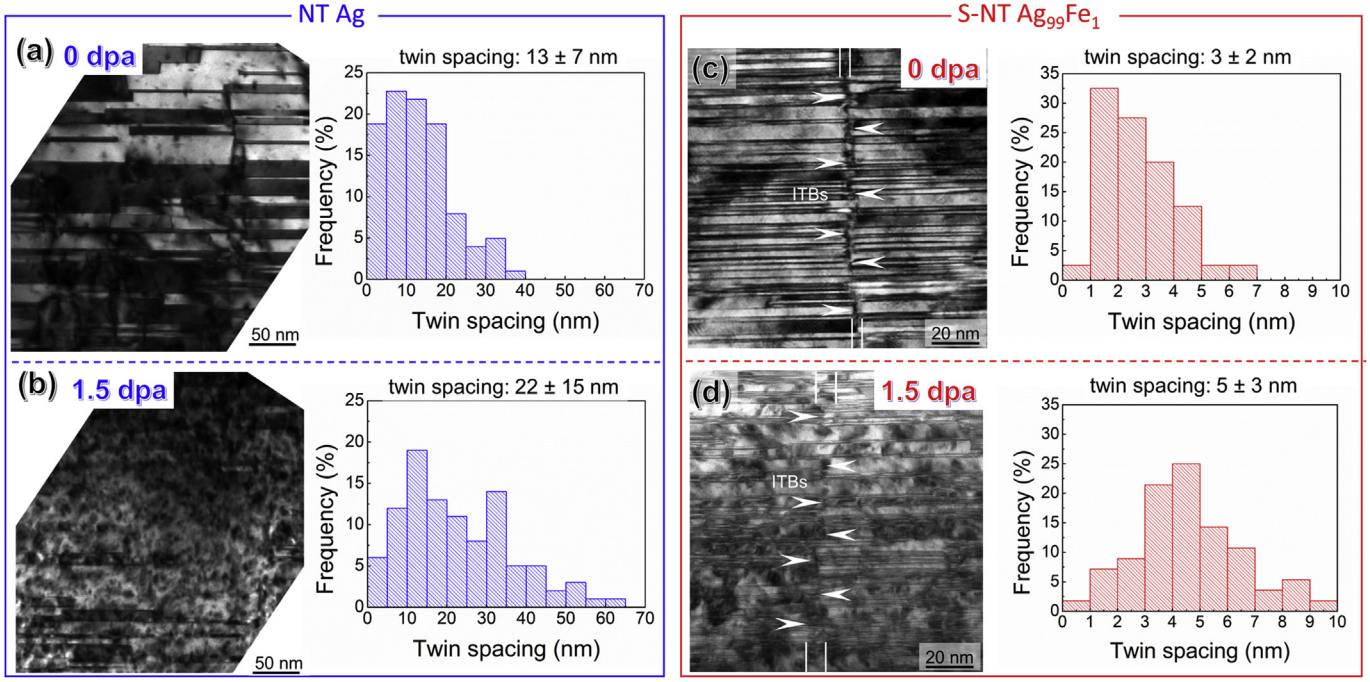

Fig. 4. XTEM images of NT Ag and S-NT $Ag_{99}Fe_1$ before and after irradiation to 1.5 dpa. (a–b) After irradiation to 1.5 dpa, numerous TBs disappeared, and the average twin spacing increased from 13 ± 7 to 22 ± 15 nm, and most ITBs at the original columnar boundaries are no longer visible after radiation. (c–d) In comparison, the TBs in irradiated S-NT $Ag_{99}Fe_1$ are much more stable. After 1.5 dpa, few TBs were removed and the average twin spacing increased slightly from 3 ± 2 to 5 ± 3 nm. The sharp ITBs became diffused and less distinguishable after irradiation. Also, the edges of CTBs became blurred due to the formation of stacking faults along CTBs.

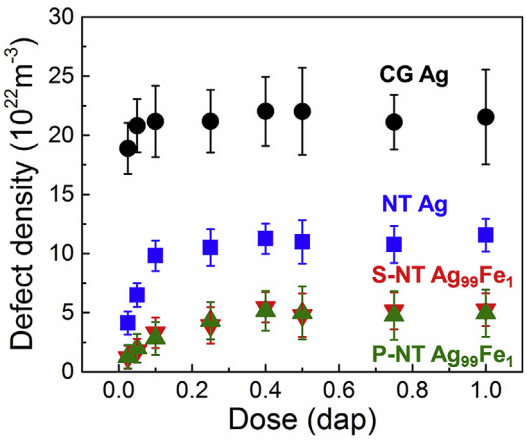

Fig. 5. The defect density evolution as a function of irradiation dose for four types of samples. The defect density in CG Ag reaches saturation at ~0.05 dpa, while defect densities in NT Ag, S-NT $Ag_{99}Fe_1$ and P-NT $Ag_{99}Fe_1$ gradually increase until 0.2 dpa, and then level off thereafter. The defect density in CG Ag reaches ~$21.5 \times 10^{22}/m^3$, and is significantly higher than that in NT Ag, ~$10.8 \times 10^{22}/m^3$. S-NT and P-NT $Ag_{99}Fe_1$ exhibit lower defect density, ~5.1 and $4.9 \times 10^{22}/m^3$, respectively.

solutes in Ag (referred to as $Ag_{99}Fe_1$), the irradiation resistance of NT Ag is largely improved. TEM characterizations show significantly improved stability of TBs against irradiation. To understand the influence of Fe solute on twin stability, DFT was used to calculate the formation energy of Fe solute in Ag at interstitial and substitutional sites.

The simulation cell has the dimension of $3 \times 3 \times 3$ units in the three <100> directions, containing 108 atoms. For Fe substitutions, the formation energy is 1.435 eV for an individual substitutional atom (as shown in Fig. 6a), 2.27 eV, 2.64 eV, 2.68 eV, and 2.72 eV for a pair of Fe substitutions that are located at the first, second, third, and fourth neighboring sites. The results clearly show the decreasing formation energy of Fe substitutional atoms at a reduced separation distance, indicating that Fe substitution atoms are likely to segregate in Ag if they can readily diffuse in FCC Ag. The formation energy of a tetrahedral (Fig. 6b) and octahedral (Fig. 6c) Fe interstitial is high, 5.307 and 4.718 eV, respectively, indicating the diffusion of Fe atom is difficult. As a result, the homogeneously deposited Fe atoms shall be uniformly distributed in Ag. This is consistent with the EDS maps shown in Suppl. Fig. 1 and Suppl. Fig. 2, which show uniformly distributed Fe before and after irradiation. It is noted that the formation energy of Ag self-

Table 1
A summary of average grain size, twin spacing (before and after irradiation), defect size and density in irradiated specimens.

	CGAg	NT Ag	S-NTAgFe	P-NTAgFe
Grain size (nm)	~5 μm	110 ± 20	110 ± 30	110 ± 30
Twin spacing (nm) Before irradiation	–	13 ± 7	3 ± 2	3 ± 2
Twin spacing (nm) After irradiation	–	22 ± 15	5 ± 3	–
Defect size (nm)	12 ± 5	7 ± 2	5 ± 2	5 ± 1
Defect density (10^{22} /m^3)	21.5 ± 0.5	10.8 ± 0.5	5.1 ± 0.3	4.9 ± 0.6

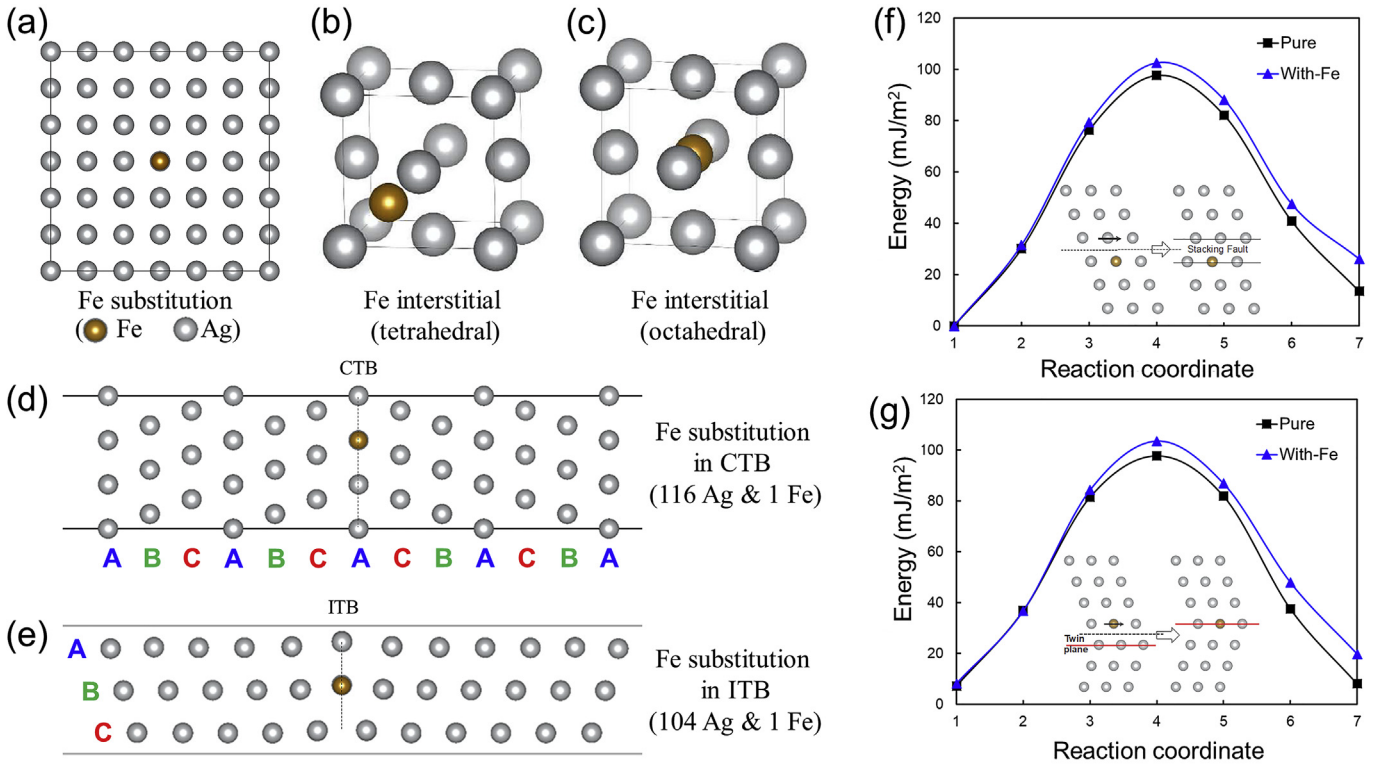

Fig. 6. (a–e) Configurations of Fe impurities in Ag at interstitial and substitutional sites at different locations used for DFT simulations. (f) Creation of an intrinsic stacking fault in Ag with and without Fe substitutional atom (via shear displacement) showing the increase of the stable stacking fault energy by 12 mJ/m^2, and the increase of unstable stacking fault energy by ~ 5 mJ/m^2. (g) Comparison of migration energy barrier for a coherent twin boundary with and without the Fe substitutional atom shows an increase of energy barrier by ~ 6 mJ/m^2 with Fe substitutional atom at the original twin boundary.

interstitials is much lower, 3.64 eV at a tetrahedral site and 3.35 eV at an octahedral site. Comparison of these energy levels indicates that Fe solutes may be preferably located at a lattice site of FCC Ag as substitutional atoms, while Ag may occupy an interstitial site.

The formation energies of Fe solutes at Σ3(111) CTBs (Fig. 6d) and Σ3(112) ITBs (Fig. 6e) were also calculated. The formation energy of an Fe substitutional atom in the CTB is 1.485 eV, higher than that in bulk, indicating that CTBs are not favorable sites for Fe atoms. At an areal density of 10 at.% Fe, the stacking fault energy of (111) planes is 26 mJ/m^2, greater than that of pure Ag, 13.51 mJ/m^2 as shown in Fig. 6f. Unlike the higher formation energy of Fe solutes in CTBs, the substitutional Fe atoms show a lower formation energy, 1.157–1.35 eV, at Σ3(112) ITBs as shown in Fig. 6e, depending on their respective positions at the ITB [42]. More importantly, the formation energy of an Fe interstitial is in the range of 1.851–1.950 eV, much lower than that in the bulk Ag. These calculations indicate that ITBs are energetically preferred sites for Fe solutes at either interstitial or substitutional positions. Correspondingly, detwinning becomes difficult because of the energy increase associated with the migration of ITBs away from the Fe solutes environment. Also, DFT calculations in Fig. 6g shows that Fe substitutional atoms increase the energy barrier for migration of twin boundaries in Ag. The effect of Fe solutes on twin stability and irradiation response of Ag can be considered from several aspects and will be discussed in details in the subsequent sections.

4.2. Formation of ultra-high-density twins in NT $Ag_{99}Fe_1$ solid solution alloys

Nanoscale growth twins have been observed in numerous monolithic metals, such as Ag [69], Cu [18,70], Ni [71], Pd [72] and Al [73,74], and their alloys [75,76]. The influence of solutes on the formation of twins has been a subject under debate [76–78]. Lu and Hellawell have proposed an “impurity-induced twinning” mechanism in their study of twin formation in Si in the casted Al-Si alloys [76]. Their study shows that the adsorption of solute atoms at monolayer steps may contribute to an alteration of the stacking sequence of {111} planes in Si, and thus tailor the formation of twins in Si. They hypothesize that growth twins are promoted in Si, when the atomic radius ratio of the solutes -to-Si exceeds 1.65. Shahani et al. have studied the twinning in Al-Si-Cu alloys, but they found neither Al nor Cu satisfies the geometrical consideration [78]. Moreover, Timpel et al. reported that the chemistry of co-segregated species rather than size effect plays a major role on the formation of twins [77]. Clearly, solute-induced twinning is a phenomenon requiring further investigation.

The formation of high-density growth twins, with an average twin spacing of several nm, in the $Ag_{99}Fe_1$ alloy can be understood from the following aspects. It has been shown that the addition of solute elements often lowers the SFE of metals and thus promotes the formation of twins [79,80]. First, although our DFT calculations show that Fe impurities will increase the SFE of Ag by about 12 mJ/m^2, compared with the SFE of pure Ag (10–20 mJ/m^2), such a moderate increase in SFE does not significantly impact the capability to form high-density growth twins in Ag. For instance, pure Cu (FCC) has a comparable SFE of ~40 mJ/m^2 and is known to have high-density growth twins in sputtered films [18,42,81]. Second, ITBs are known to be the sources for detwinning. Our DFT calculations show that the formation energy of Fe at ITB at either interstitial or substitutional positions are lower than Fe solute in bulk Ag lattices as shown in Table 2. Correspondingly, detwinning

Table 2
Formation energies of Fe impurities in Ag as interstitials and substitutions with respect to different locations.

	Bulk		CTB	ITB	
	interstitial	substitution	substitution	interstitial	substitution
Formation energy of Fe(eV)	5.307(tetra) 4.718(octa)	1.435	1.485	1.851–1.950	1.157–1.350

becomes difficult because of the energy increase associated with the migration of ITBs away from the Fe solutes. Third, the average spacing between Fe atoms in the $Ag_{99}Fe_1$ alloy is ~2 nm, comparable to the average twin spacing (3 ± 2 nm), indicating that Fe impurity has also pinned the migration of CTBs and thus significantly stabilize the fine twins.

4.3. Significantly enhanced irradiation stability of TBs in NT $Ag_{99}Fe_1$

Prior studies have shown that TBs are mobile under stress (deformation) [82] and radiation [39,47,82,83]. ITB segments consist of 1/6<112> Shockley partial dislocations on consecutive {111} planes. *In situ* nanoindentation in TEM and molecular dynamics simulations show that ITBs are mobile during deformation, a phenomenon often referred to as detwinning [82]. The driving force for detwinning is the reduction in TB energy. Detwinning has also been reported in irradiated NT Cu [39,47,82] and NT Ag [83]. In general, CTBs can actively engage in defect clusters and form a series of tiny ITBs steps. These ITBs are highly mobile and thus promote detwinning.

The columnar boundaries in NT Ag and S-NT $Ag_{99}Fe_1$ are predominantly ITBs [69]. After irradiation to 1.5 dpa, TBs in NT Ag detwin significantly. In comparison, the ITBs in S-NT $Ag_{99}Fe_1$ are highly stable. Previous studies show that detwinning velocity in NT Cu increases rapidly for fine twins (inversely proportional to the twin thickness) [39,47]. In the current study, however, fine twins, ~3 nm in NT $Ag_{99}Fe_1$ remain stable. The superior stability of TBs in irradiated NT $Ag_{99}Fe_1$ can be interpreted from the following perspectives.

First, as shown in Table 2, Fe solutes have a lower formation energy, 1.157 eV, when located at Σ3(112) ITBs comparing to that at Σ3(111) CTBs (1.485 eV) or in the bulk lattice (1.372 eV), indicating that ITBs are energetically preferred sites for Fe solutes. If ITBs migrate, Fe solute will be left in the bulk, increasing the total energy of the system. Consequently, the migration of ITBs is prohibited due to the existence of Fe solutes.

Second, the solute drag effect may also retard the migration of ITBs. Solute drag effect on GB mobility has been extensively investigated [84–89]. Lücke and Detert [84] proposed that GB mobility M can be expressed as [90],

$$M = \frac{D}{kT}\frac{1}{nCe^{-E/kT}}, \quad (2)$$

where D is the diffusivity of solute atoms, n is the number of solute atoms per unit area of the boundary, C is the average concentration of solute atoms, and E is the boundary–solute interaction energy, i.e., the heat of segregation. Clearly, the mobility of GB is proportional to the diffusivity of solute atoms and inversely proportional to the concentration of solute atoms.

Borovikov et al. have studied the drag effect of Ag solutes in Cu on TB stability by MD simulations [90]. Their modeling study suggests that the presence of Ag solutes, 0.2–0.5 at.%, significantly resists the migration of ITBs. The migration rate of ITBs is twin-thickness-dependent, and the ITBs migrate 14 times faster in pure Cu than that with Ag solutes. Also, ITBs migrate smoothly in the pure Cu, whereas the ITB movement becomes jerky in the presence of Ag solutes. Zhang et al., have also pointed out the importance of solute drag effect on the enhanced high-temperature stability of TBs in NT Cu contains 0.5 at% Fe precipitates at GBs [16]. Our DFT calculations show that Fe solute increases the energy barriers for the migration of TBs in Ag, and thus may stabilize TBs during radiation.

Third, Fe has an atomic radius of 1.56 Å, smaller than Ag, 1.65 Å. Smaller solute atoms introduce tensile stress field and thus may trap dislocations, such as mobile Shockley partials. Therefore, such Fe solutes may slow down the migration of Shockley partial dislocations on the ITBs, and thus retard the migration of ITBs. Additionally, it has been proposed that the interaction of dislocation loops with Shockley partials (on ITBs) may lead to sessile Frank partials [48]. It is likely that the Fe solutes may stabilize Frank partials, making them difficult to evolve and thus stabilize ITBs.

Finally, it is worth mentioning that the formation of a high density of SFs along TBs is normally observed in NT Ag and Cu after irradiation [47,91]. Fe solute atoms may facilitate the formation of SFs along CTBs during radiation. Such a phenomenon can be seen in Fig. 4d where TBs in NT $Ag_{99}Fe_1$ became blurred (decorated with SFs) after irradiation.

4.4. The integration of Fe solutes and CTB-ITB networks to enhance radiation tolerance

4.4.1. Role of CTBs on irradiation tolerance

It has been known that NT metals have enhanced radiation tolerance compared to their bulk counterparts. The current study confirmed that NT Ag and $Ag_{99}Fe_1$ indeed have significantly improved radiation tolerance than CG Ag. Although there are studies that show CTBs may be ineffective defect sinks comparing to other HAGBs [12,37], there is increasing evidence that shows CTBs can actively engage in defect capture and annihilation during irradiation. For instance, both MD simulations and *in situ* radiation studies show that CTBs interact with and destruct SFTs [15,17,18,38,92]. CTBs also change their geometry to accommodate dislocation loops and facilitate the transportation of interstitials along CTBs to locations where vacancy concentration is high, and thus promote vacancy-interstitial recombinations [17]. Recent studies on NT Ag have also shown the defect-CTB interactions lead to the existence of twin boundary affected zone (TBAZ), where the time accumulative defect concentration is lower near CTBs [17]. In addition, the distribution of defects has been revealed to be twin-thickness (spacing between CTBs) dependent [46]. These studies confirm that CTBs are indeed effective sinks in irradiated metals.

The current study shows that NT Ag and NT $Ag_{99}Fe_1$ have similar columnar grain size, ~110 nm, but NT $Ag_{99}Fe_1$ has a much smaller twin spacing, 3 ± 2 nm, comparing to that of NT Ag, 13 ± 7 nm. Irradiated $Ag_{99}Fe_1$ has 50% less defects than NT Ag, as well as a smaller average defect size. Such a drastic reduction of defect density and a moderate decrease in defect dimension are related to the much smaller average twin thickness in NT $Ag_{99}Fe_1$, lending further evidence on the role of CTBs on the alleviation of radiation damage. The dislocation loop size in NT $Ag_{99}Fe_1$ is comparable to their average twin spacing, indicating that nanotwins may have

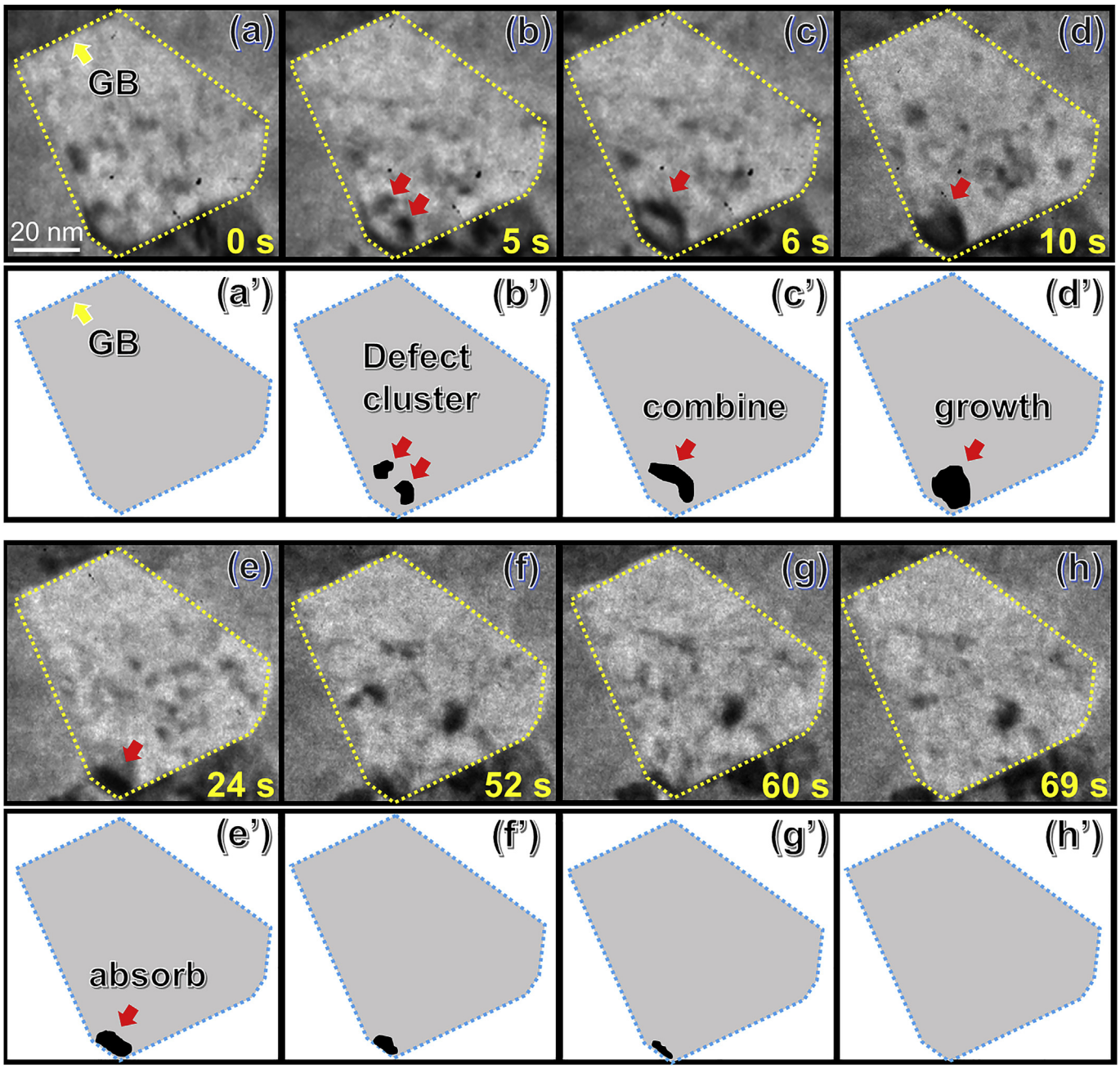

Fig. 7. *In situ* TEM video snapshots (a–h) showing representative defect capture events by a grain boundary (GB) in P-NT $Ag_{99}Fe_1$ over ~ 0.15 dpa (~69 s) (see Supplementary Video 1). (a) The boundary of a grain is indicated by yellow dotted line. (b) Two defect clusters appeared at 5 s as indicated by red arrows. (c) They combined into a large cluster at 6 s. (d) The defect evolved further into a large defect cluster. (e) The large defect cluster was gradually absorbed by the GB at 24 s and became smaller (f–g). (h) Finally, the defect cluster was removed by the GB. The corresponding schematic diagrams of the defect-GB interaction events described in (a–h) are shown in (a'-h'). . (For interpretation of the references to colour in this figure legend, the reader is referred to the Web version of this article.)

significantly suppressed the growth of defect clusters during radiation.

4.4.2. Columnar grain boundary and ITBs as defect sinks in irradiated NT metals

NT Ag and NT $Ag_{99}Fe_1$ have abundant columnar GBs. *In situ* TEM snapshots (Fig. 7) show representative defect capture events by a grain boundary in P-NT $Ag_{99}Fe_1$ over ~0.15 dpa (~69 s) (see Supplementary Video 1). The boundary of a grain is indicated by the yellow dotted line (Fig. 7a). After 5s, two defect clusters near a GB appeared as indicated by red arrows (Fig. 7b). By 6s, they combined into a large cluster that grew further (Fig. 7c–d) and remained in contact with the GB. The large defect cluster was gradually absorbed by the GB at 24 s and continuously shrank (Fig. 7e–g). Finally, the defect cluster was nearly completely removed by the GB at 69 s (Fig. 7h). The corresponding schematic diagrams of the defect-GB interaction events are shown in Fig. 7a'-h'. Such a defect cluster could be a vacancy loop, and the absorption of a large vacancy loop by GBs is a sluggish process as it involves substantial diffusion of atoms along GBs. There are also prior studies that show ITBs as effective defect sinks [93,94]. And it has been shown that ITBs can sometimes recover after interactions with dislocation loops [48].

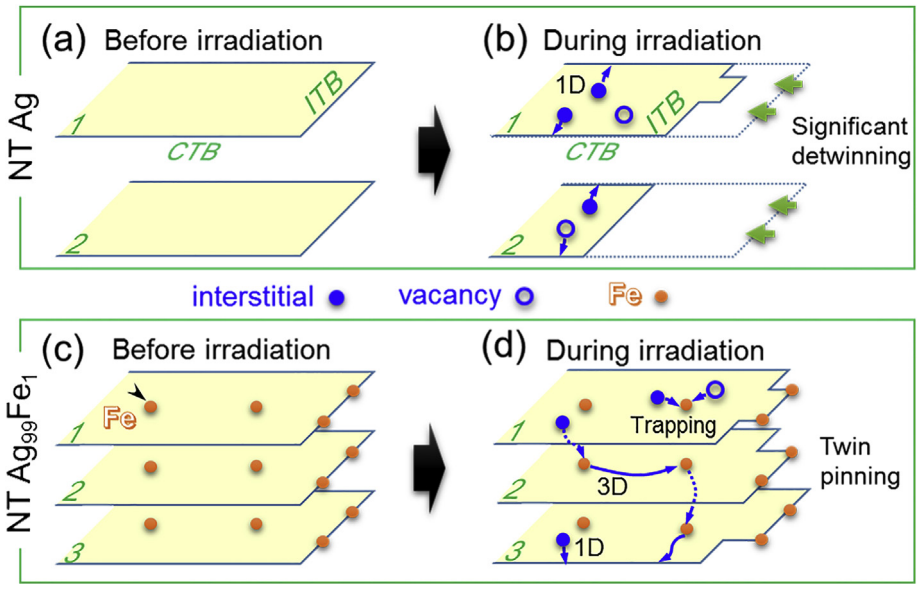

Fig. 8. Schematics illustrate the different irradiation responses between NT Ag and S-NT $Ag_{99}Fe_1$. (a–b) Irradiation of NT Ag leads to significant detwinning. Besides, irradiation-induced point defects in NT Ag migrate fast towards TBs and then along TBs in a 1D/2D manner. (c–d) During irradiation of NT $Ag_{99}Fe_1$, ITBs are pinned by Fe solutes and detwinning is significantly suppressed. In addition, as shown in (d), a Ag self-interstitial atom on plane 1 can migrate to an Fe solute on plane 2, then it may migrate between Fe solutes on the plane 2, before it jumps again to another Fe solute atom on plane 3. Hence, the existence of Fe solute may change the Ag self-interstitials from 1D/2D to a more random 3D migration behavior. Note that Fe solutes introduce tensile stress (as Fe solutes have smaller atomic radius than Ag atoms), making Fe solutes preferential sites for interstitials.

ITBs not only capture large defect clusters, but also effectively transport point defects. Prior studies on Kr ion irradiated NT Cu with nanovoids show that Shockley partials at ITB steps can effectively transport interstitials to GBs where they can be annihilated by nanovoids [42]. It is worth mentioning that the CTBs in as-deposited NT Ag and AgFe films already contain some ITB steps. During radiation, the interaction of defect clusters with CTBs leads to rapid increase in the population of ITB steps. These ITB steps can rapidly transport point defects on CTBs, making CTBs effective defect sinks.

Supplementary video related to this article can be found at https://doi.org/10.1016/j.actamat.2018.03.052.

4.4.3. Role of Fe solute atoms on improved irradiation tolerance

Classical solute drag effect assumes that solute atoms migrate together with GBs or dislocations and consequently may segregate in the form of precipitates. However, EDS mapping did not reveal segregation of Fe solutes near TBs in irradiated NT $Ag_{99}Fe_1$, indicating that solute atoms did not massively travel along with ITBs or Shockley partials. The significance of Fe solutes on radiation tolerance of NT $Ag_{99}Fe_1$ can be interpreted from several perspectives.

First, Fe solutes are preferably located at lattice sites of FCC Ag as substitutional atoms, while Ag will be replaced to occupy an interstitial site. Therefore, during irradiation, the substitutional Fe atoms alter the evolution of irradiation-induced point defects, such as Ag self-interstitial atoms (SIAs). In general, Ag SIAs may migrate rapidly in a 1D/2D fashion on their habit planes and TBs in the absence of Fe. However, Ag SIAs may migrate to Fe solutes on neighboring planes (due to the existence of tensile stress near Fe solutes). Thus, Fe solute may promote a more complicated 3D migration of Ag SIAs as shown schematically in Fig. 8. Consequently, the migration of interstitials is slowed down, alleviating the radiation-induced rapid increase of defect cluster density. Second, Fe solutes may facilitate the recombination of opposite types of point defects, a phenomenon that has been reported previously [49–53]. Fe has smaller atomic radius than Ag, and thus a tensile stress field may arise around substitutional Fe atoms, making Fe solutes preferential sites to attract interstitials (As shown in Fig. 8). Although Fe solute may not eliminate interstitials due to the limited excess free volume, they increase an interstitial's dwelling time, promoting the interstitial to recombine with nearby vacancies. The average separation distance among these Fe solutes is only ~2 nm, making them effective to prohibit preferential segregation of vacancy and interstitial clusters. Finally, as Fe solutes stabilize TBs significantly, TBs can effectively engage and decompose defect clusters into point defects along TBs. Fe solutes facilitate the recombination of these point defects. Hence, Fe solutes and CTBs and ITBs form an effective defect sink network, which leads to remarkable radiation tolerance of NT $Ag_{99}Fe_1$ alloys.

5. Conclusion

In situ heavy ion irradiation studies show drastically improved irradiation stability of twin boundaries in NT $Ag_{99}Fe_1$ compared with NT Ag. Moreover, NT $Ag_{99}Fe_1$ has much smaller defect size and lower defect density than NT Ag. DFT simulations show that Fe solutes significantly improve the energy barrier for migration of twin boundaries in Ag. The substitutional Fe solutes improve irradiation resistance of Ag by changing the migration and aggregation behavior of irradiation-induced point defects from 1D/2D to 3D and accelerating the recombination of interstitials and vacancy through trapping and detrapping processes. The uniformly distributed Fe solutes integrate nicely into the CTB-ITB networks to capture and promote recombination of opposite point defects and stabilize ITBs, and the combinations of solute-TB networks lead to outstanding radiation tolerance in NT alloys.

Acknowledgement

We acknowledge financial support by NSF-DMR-Metallic Materials and Nanostructures Program under grant no. 1643915. CF is supported by NSF-CMMI-1728419. HW acknowledges the support from the U.S. Office of Naval Research (N00014-17-1-2087). We also acknowledge the use of microscopes at the Microscopy and

Imaging Center at Texas A&M University and the DoE Center for Integrated Nanotechnologies managed by Los Alamos National Laboratory. The IVEM facility at Argonne National Laboratory is supported by DOE-Office of Nuclear Energy. The DFT calculation was completed utilizing the Holland Computing Center of the University of Nebraska, which receives support from the Nebraska Research Initiative.

Appendix A. Supplementary data

Supplementary data related to this article can be found at https://doi.org/10.1016/j.actamat.2018.03.052.

References

[1] S.J. Zinkle, 1.03-Radiation-Induced effects on microstructure* A2-Konings, in: J.M. Rudy (Ed.), Comprehensive Nuclear Materials, Elsevier, Oxford, 2012, pp. 65–98.
[2] S.J. Zinkle, in: Materials Issues for Generation IV Systems, Springer, Netherlands, 2008, pp. 227–244.
[3] D. Norris, The use of the high voltage electron microscope to simulate fast neutron-induced void swelling in metals, J. Nucl. Mater. 40 (1971) 66–76.
[4] L.K. Mansur, Void swelling in metals and alloys under irradiation: an assessment of the theory, Nucl. Technol. 40 (1978) 5–34.
[5] R.W. Grimes, R.J.M. Konings, L. Edwards, Greater tolerance for nuclear materials, Nat. Mater. 7 (2008) 683–685.
[6] G.R. Odette, M.J. Alinger, B.D. Wirth, Recent developments in irradiation-resistant steels, Annu. Rev. Mater. Res. 38 (2008) 471–503.
[7] K.Y. Yu, Y. Chen, J. Li, Y. Liu, H. Wang, M.A. Kirk, M. Li, X. Zhang, Measurement of heavy ion irradiation induced in-plane strain in patterned face-centered-cubic metal films: an in situ study, Nano Lett. 16 (2016) 7481–7489.
[8] E. Little, D. Stow, Void-swelling in irons and ferritic steels: II. An experimental survey of materials irradiated in a fast reactor, J. Nucl. Mater. 87 (1979) 25–39.
[9] S.A. Maloy, M.R. James, G. Willcutt, W.F. Sommer, M. Sokolov, L.L. Snead, M.L. Hamilton, F. Garner, The mechanical properties of 316L/304L stainless steels, Alloy 718 and Mod 9Cr–1Mo after irradiation in a spallation environment, J. Nucl. Mater. 296 (2001) 119–128.
[10] T.D. Shen, S. Feng, M. Tang, J.A. Valdez, Y. Wang, K.E. Sickafus, Enhanced radiation tolerance in nanocrystalline MgGa2O4, Appl. Phys. Lett. 90 (2007) 263115.
[11] K.Y. Yu, Y. Liu, C. Sun, H. Wang, L. Shao, E.G. Fu, X. Zhang, Radiation damage in helium ion irradiated nanocrystalline Fe, J. Nucl. Mater. 425 (2012) 140–146.
[12] W.Z. Han, M.J. Demkowicz, E.G. Fu, Y.Q. Wang, A. Misra, Effect of grain boundary character on sink efficiency, Acta Mater. 60 (2012) 6341–6351.
[13] M. Song, Y.D. Wu, D. Chen, X.M. Wang, C. Sun, K.Y. Yu, Y. Chen, L. Shao, Y. Yang, K.T. Hartwig, X. Zhang, Response of equal channel angular extrusion processed ultrafine-grained T91 steel subjected to high temperature heavy ion irradiation, Acta Mater. 74 (2014) 285–295.
[14] M.A. Tschopp, K. Solanki, F. Gao, X. Sun, M.A. Khaleel, M. Horstemeyer, Probing grain boundary sink strength at the nanoscale: energetics and length scales of vacancy and interstitial absorption by grain boundaries in α-Fe, Phys. Rev. B 85 (2012) 064108.
[15] K.Y. Yu, D. Bufford, C. Sun, Y. Liu, H. Wang, M.A. Kirk, M. Li, X. Zhang, Removal of stacking-fault tetrahedra by twin boundaries in nanotwinned metals, Nat. Commun. 4 (2013) 1377.
[16] X. Zhang, A. Misra, Superior thermal stability of coherent twin boundaries in nanotwinned metals, Scripta Mater. 66 (2012) 860–865.
[17] J. Li, K.Y. Yu, Y. Chen, M. Song, H. Wang, M.A. Kirk, M. Li, X. Zhang, In situ study of defect migration kinetics and self-healing of twin boundaries in heavy ion irradiated nanotwinned metals, Nano Lett. 15 (2015) 2922–2927.
[18] Y. Chen, J. Li, K.Y. Yu, H. Wang, M.A. Kirk, M. Li, X. Zhang, In situ studies on radiation tolerance of nanotwinned Cu, Acta Mater. 111 (2016) 148–156.
[19] C. Fan, Y. Chen, J. Li, J. Ding, H. Wang, X. Zhang, Defect evolution in heavy ion irradiated nanotwinned Cu with nanovoids, J. Nucl. Mater. 496 (2017) 293–300.
[20] C. Sun, B.P. Uberuaga, L. Yin, J. Li, Y. Chen, M.A. Kirk, M. Li, S.A. Maloy, H. Wang, C. Yu, X. Zhang, Resilient ZnO nanowires in an irradiation environment: an in situ study, Acta Mater. 95 (2015) 156–163.
[21] J. Li, C. Fan, J. Ding, S. Xue, Y. Chen, Q. Li, H. Wang, X. Zhang, In situ heavy ion irradiation studies of nanopore shrinkage and enhanced radiation tolerance of nanoporous Au, Sci. Rep. 7 (2017) 39484.
[22] E.M. Bringa, J.D. Monk, A. Caro, A. Misra, L. Zepeda-Ruiz, M. Duchaineau, F. Abraham, M. Nastasi, S.T. Picraux, Y.Q. Wang, D. Farkas, Are nanoporous materials radiation resistant? Nano Lett. 12 (2012) 3351–3355.
[23] J. Li, Y. Chen, H. Wang, X. Zhang, In situ study on enhanced heavy ion irradiation tolerance of porous Mg, Scripta Mater. 144 (2018) 13–17.
[24] J. Li, C. Fan, Q. Li, H. Wang, X. Zhang, In situ studies on irradiation resistance of nanoporous Au through temperature-jump tests, Acta Mater. 143 (2018) 30–42.
[25] Y. Chen, Y. Liu, E.G. Fu, C. Sun, K.Y. Yu, M. Song, J. Li, Y.Q. Wang, H. Wang, X. Zhang, Unusual size-dependent strengthening mechanisms in helium ion-irradiated immiscible coherent Cu/Co nanolayers, Acta Mater. 84 (2015) 393–404.
[26] M.J. Demkowicz, A. Misra, A. Caro, The role of interface structure in controlling high helium concentrations, Curr. Opin. Solid State Mater. Sci. 16 (2012) 101–108.
[27] Q.M. Wei, N. Li, N. Mara, M. Nastasi, A. Misra, Suppression of irradiation hardening in nanoscale V/Ag multilayers, Acta Mater. 59 (2011) 6331–6340.
[28] K.Y. Yu, Z. Fan, Y. Chen, M. Song, Y. Liu, H. Wang, M.A. Kirk, M. Li, X. Zhang, In situObservation of defect annihilation in Kr ion-irradiated bulk Fe/Amorphous-Fe2Zr nanocomposite alloy, Materials Research Letters 3 (2014) 35–42.
[29] Y. Chen, N. Li, D.C. Bufford, J. Li, K. Hattar, H. Wang, X. Zhang, In situ study of heavy ion irradiation response of immiscible Cu/Fe multilayers, J. Nucl. Mater. 475 (2016) 274–279.
[30] H. Wang, R. Araujo, J.G. Swadener, Y.Q. Wang, X. Zhang, E.G. Fu, T. Cagin, Ion irradiation effects in nanocrystalline TiN coatings, Nucl. Instrum. Methods Phys. Res. Sect. B Beam Interact. Mater. Atoms 261 (2007) 1162–1166.
[31] X.-M. Bai, A.F. Voter, R.G. Hoagland, M. Nastasi, B.P. Uberuaga, Efficient annealing of radiation damage near grain boundaries via interstitial emission, Science 327 (2010) 1631–1634.
[32] T.D. Shen, Radiation tolerance in a nanostructure: is smaller better? Nucl. Instrum. Methods Phys. Res. Sect. B Beam Interact. Mater. Atoms 266 (2008) 921–925.
[33] B.N. Singh, M. Eldrup, S.J. Zinkle, S.I. Golubov, On grain-size-dependent void swelling in pure copper irradiated with fission neutrons, Philos. Mag. A 82 (2002) 1137–1158.
[34] B.N. Singh, Effect of grain size on void formation during high-energy electron irradiation of austenitic stainless steel, Phil. Mag. 29 (1974) 25–42.
[35] C. Sun, M. Song, K. Yu, Y. Chen, M. Kirk, M. Li, H. Wang, X. Zhang, In situ evidence of defect cluster absorption by grain boundaries in Kr ion irradiated nanocrystalline Ni, Metall. Mater. Trans. 44 (2013) 1966–1974.
[36] O. El-Atwani, J. Nathaniel II, A. Leff, J. Baldwin, K. Hattar, M. Taheri, Evidence of a temperature transition for denuded zone formation in nanocrystalline Fe under He irradiation, Materials Research Letters (2016) 1–6.
[37] M.J. Demkowicz, O. Anderoglu, X. Zhang, A. Misra, The influence of ∑3 twin boundaries on the formation of radiation-induced defect clusters in nanotwinned Cu, J. Mater. Res. 26 (2011) 1666–1675.
[38] M. Niewczas, R.G. Hoagland, Molecular dynamic studies of the interaction of a/6⟨112⟩ Shockley dislocations with stacking fault tetrahedra in copper. Part II: intersection of stacking fault tetrahedra by moving twin boundaries, Phil. Mag. 89 (2009) 727–746.
[39] C. Fan, J. Li, Z. Fan, H. Wang, X. Zhang, In situ studies on the irradiation-induced twin boundary-defect interactions in Cu, Metall. Mater. Trans. 48 (2017) 5172–5180.
[40] N. Li, J. Wang, A. Misra, X. Zhang, J.Y. Huang, J.P. Hirth, Twinning dislocation multiplication at a coherent twin boundary, Acta Mater. 59 (2011) 5989–5996.
[41] Y. Chen, X. Zhang, J. Wang, Radiation enhanced absorption of Frank loops by nanovoids in Cu, Jom-Us 68 (2016) 235–241.
[42] Y. Chen, K.Y. Yu, Y. Liu, S. Shao, H. Wang, M. Kirk, J. Wang, X. Zhang, Damage-tolerant nanotwinned metals with nanovoids under radiation environments, Nat. Commun. 6 (2015).
[43] X.M. Bai, A.F. Voter, R.G. Hoagland, M. Nastasi, B.P. Uberuaga, Efficient annealing of radiation damage near grain boundaries via interstitial emission, Science 327 (2010) 1631–1634.
[44] B.n. Singh, Foreman, Calculated grain size-dependent vacancy supersaturation and its effect on void formation, Philosophical magazine 29 (1974) 847–858.
[45] C. Jiang, N. Swaminathan, J. Deng, D. Morgan, I. Szlufarska, Effect of grain boundary stresses on sink strength, Materials Research Letters 2 (2014) 100–106.
[46] J. Li, Y. Chen, H. Wang, X. Zhang, In situ studies on twin-thickness-dependent distribution of defect clusters in heavy ion-irradiated nanotwinned Ag, Metall. Mater. Trans. 48 (2017) 1466–1473.
[47] Y. Chen, H. Wang, M. Kirk, M. Li, J. Wang, X. Zhang, Radiation induced detwinning in nanotwinned Cu, Scripta Mater. 130 (2017) 37–41.
[48] K.Y. Yu, D. Bufford, F. Khatkhatay, H. Wang, M.A. Kirk, X. Zhang, In situ studies of irradiation-induced twin boundary migration in nanotwinned Ag, Scripta Mater. 69 (2013) 385–388.
[49] D.J. Hepburn, E. MacLeod, G.J. Ackland, Transition metal solute interactions with point defects in fcc iron from first principles, Phys. Rev. B 92 (2015) 014110.
[50] S. Zhao, G. Velisa, H. Xue, H. Bei, W.J. Weber, Y. Zhang, Suppression of vacancy cluster growth in concentrated solid solution alloys, Acta Mater. 125 (2017) 231–237.
[51] Fundamental Aspects of Radiation Damage in Metals. Proceedings of an International Conference, Gatlinburg, Tennessee, October 6–10, 1975, distributed by the Office of Scientific and Technical Information, U.S. Dept. of Energy, Oak Ridge, Tenn, Oak Ridge, Tenn, 1975.
[52] E.A. Little, Development of radiation resistant materials for advanced nuclear power plant, Mater. Sci. Technol. 22 (2006) 491–518.
[53] E.A. Little, Neutron-irradiation hardening in irons and ferritic steels, Int. Met. Rev. 21 (1976) 25–60.
[54] W. Mansel, G. Vogl, Fast neutron radiation damage in aluminium studied by interstitial trapping at 57 Co Mossbauer atoms, J. Phys. F Met. Phys. 7 (1977)

253.
[55] A.V. Barashev, S.I. Golubov, Unlimited damage accumulation in metallic materials under cascade-damage conditions, Phil. Mag. 89 (2009) 2833–2860.
[56] X. Zhang, K. Hattar, Y. Chen, L. Shao, J. Li, C. Sun, K. Yu, N. Li, M.L. Taheri, H. Wang, J. Wang, M. Nastasi, Radiation damage in nanostructured materials, Prog. Mater. Sci. 96 (2018) 217–321 in press.
[57] M. Kiritani, Story of stacking fault tetrahedra, Mater. Chem. Phys. 50 (1997) 133–138.
[58] M. Hiratani, H.M. Zbib, B.D. Wirth, Interaction of glissile dislocations with perfect and truncated stacking-fault tetrahedra in irradiated metals, Philos. Mag. A 82 (2002) 2709–2735.
[59] Y. Matsukawa, S.J. Zinkle, Dynamic observation of the collapse process of a stacking fault tetrahedron by moving dislocations, J. Nucl. Mater. 329–333 (Part B) (2004) 919–923.
[60] B.N. Singh, S.I. Golubov, H. Trinkaus, D.J. Edwards, M. Eldrup, Review: evolution of stacking fault tetrahedra and its role in defect accumulation under cascade damage conditions, J. Nucl. Mater. 328 (2004) 77–87.
[61] B.P. Uberuaga, R.G. Hoagland, A.F. Voter, S.M. Valone, Direct transformation of vacancy voids to stacking fault tetrahedra, Phys. Rev. Lett. 99 (2007) 135501.
[62] J. Wang, O. Anderoglu, J.P. Hirth, A. Misra, X. Zhang, Dislocation structures of Sigma 3 {112} twin boundaries in face centered cubic metals, Appl. Phys. Lett. 95 (2009), 021908–021903.
[63] I.J. Beyerlein, X. Zhang, A. Misra, Growth twins and deformation twins in metals, Annu. Rev. Mater. Res. 44 (2014), 329–363.
[64] G. Kresse, J. Furthmüller, Efficiency of ab-initio total energy calculations for metals and semiconductors using a plane-wave basis set, Comput. Mater. Sci. 6 (1996) 15–50.
[65] G. Kresse, J. Hafner, Ab initio, Phys. Rev. B 47 (1993) 558–561.
[66] J.P. Perdew, J.A. Chevary, S.H. Vosko, K.A. Jackson, M.R. Pederson, D.J. Singh, C. Fiolhais, Atoms, molecules, solids, and surfaces: applications of the generalized gradient approximation for exchange and correlation, Phys. Rev. B 46 (1992) 6671–6687.
[67] G. Kresse, J. Hafner, Norm-conserving and ultrasoft pseudopotentials for first-row and transition elements, J. Phys. Condens. Matter 6 (1994) 8245.
[68] J.P. Perdew, in: P. Ziesche, H. Eschrig (Eds.), Electronic Structure of Solids, Akademie Verlag, Berlin, 1991.
[69] D. Bufford, H. Wang, X. Zhang, High strength, epitaxial nanotwinned Ag films, Acta Mater. 59 (2011) 93–101.
[70] A. Hodge, T. Furnish, C. Shute, Y. Liao, X. Huang, C. Hong, Y. Zhu, T. Barbee Jr., J. Weertman, Twin stability in highly nanotwinned Cu under compression, torsion and tension, Scripta Mater. 66 (2012) 872–877.
[71] X. Wu, Y.T. Zhu, M.W. Chen, E. Ma, Twinning and stacking fault formation during tensile deformation of nanocrystalline Ni, Scripta Mater. 54 (2006) 1685–1690.
[72] H. Idrissi, B. Wang, M.S. Colla, J.P. Raskin, D. Schryvers, T. Pardoen, Ultrahigh strain hardening in thin palladium films with nanoscale twins, Adv. Mater. 23 (2011) 2119–2122.
[73] S. Xue, Z. Fan, Y. Chen, J. Li, H. Wang, X. Zhang, The formation mechanisms of growth twins in polycrystalline Al with high stacking fault energy, Acta Mater. 101 (2015) 62–70.
[74] D. Bufford, Y. Liu, Y. Zhu, Z. Bi, Q.X. Jia, H. Wang, X. Zhang, Formation mechanisms of high-density growth twins in aluminum with high Stacking-fault energy, Materials Research Letters 1 (2013) 51–60.
[75] X. Zhang, A. Misra, H. Wang, M. Nastasi, J. Embury, T. Mitchell, R. Hoagland, J. Hirth, Nanoscale-twinning-induced strengthening in austenitic stainless steel thin films, Appl. Phys. Lett. 84 (2004) 1096–1098.
[76] S.-Z. Lu, A. Hellawell, The mechanism of silicon modification in aluminum-silicon alloys: impurity induced twinning, Metallurgical Transactions A 18 (1987) 1721–1733.
[77] M. Timpel, N. Wanderka, R. Schlesiger, T. Yamamoto, N. Lazarev, D. Isheim, G. Schmitz, S. Matsumura, J. Banhart, The role of strontium in modifying aluminium–silicon alloys, Acta Mater. 60 (2012) 3920–3928.
[78] A.J. Shahani, E.B. Gulsoy, S.O. Poulsen, X. Xiao, P.W. Voorhees, Twin-mediated crystal growth: an enigma resolved, Sci. Rep. 6 (2016) 28651.
[79] P.C.J. Gallagher, The influence of alloying, temperature, and related effects on the stacking fault energy, Metallurgical Transactions 1 (1970) 2429–2461.
[80] Y.C. Liu, P.C.J. Gallagher, Analytical expressions for the composition dependence of stacking fault energies and probabilities in binary silver systems, J. Appl. Phys. 42 (1971) 3322–3328.
[81] O. Anderoglu, A. Misra, H. Wang, F. Ronning, M. Hundley, X. Zhang, Epitaxial nanotwinned Cu films with high strength and high conductivity, Appl. Phys. Lett. 93 (2008) 083108.
[82] J. Wang, N. Li, O. Anderoglu, X. Zhang, A. Misra, J.Y. Huang, J.P. Hirth, Detwinning mechanisms for growth twins in face-centered cubic metals, Acta Mater. 58 (2010) 2262–2270.
[83] L. Liu, J. Wang, S.K. Gong, S.X. Mao, High resolution transmission electron microscope observation of zero-strain deformation twinning mechanisms in Ag, Phys. Rev. Lett. 106 (2011) 175504.
[84] K. Lücke, K. Detert, A quantitative theory of grain-boundary motion and recrystallization in metals in the presence of impurities, Acta Metall. 5 (1957) 628–637.
[85] K. Tapasa, D.J. Bacon, N.O. Yu, Computer simulation of dislocation–solute interaction in dilute Fe–Cu alloys, Model. Simulat. Mater. Sci. Eng. 14 (2006) 1153.
[86] M.I. Mendelev, D.J. Srolovitz, W. E, Grain-boundary migration in the presence of diffusing impurities: simulations and analytical models, Philos. Mag. A 81 (2001) 2243–2269.
[87] A. Michels, C.E. Krill, H. Ehrhardt, R. Birringer, D.T. Wu, Modelling the influence of grain-size-dependent solute drag on the kinetics of grain growth in nanocrystalline materials, Acta Mater. 47 (1999) 2143–2152.
[88] J.F. Nie, Y.M. Zhu, J.Z. Liu, X.Y. Fang, Periodic segregation of solute atoms in fully coherent twin boundaries, Science 340 (2013) 957.
[89] C.C. Koch, R.O. Scattergood, K.A. Darling, J.E. Semones, Stabilization of nanocrystalline grain sizes by solute additions, J. Mater. Sci. 43 (2008) 7264–7272.
[90] V. Borovikov, M.I. Mendelev, A.H. King, Effects of solutes on the thermal stability of nanotwinned materials, Phil. Mag. 94 (2014) 2875–2885.
[91] Y. Liu, Y. Chen, K.Y. Yu, H. Wang, J. Chen, X. Zhang, Stacking fault and partial dislocation dominated strengthening mechanisms in highly textured Cu/Co multilayers, Int. J. Plast. 49 (2013) 152–163.
[92] Q. Guo, P. Landau, P. Hosemann, Y. Wang, J.R. Greer, Helium implantation effects on the compressive response of Cu nanopillars, Small 9 (2013) 691–696.
[93] N. Li, J. Wang, Y. Wang, Y. Serruys, M. Nastasi, A. Misra, Incoherent twin boundary migration induced by ion irradiation in Cu, J. Appl. Phys. 113 (2013) 023508.
[94] Q. Lu, Q. Su, F. Wang, C. Zhang, Y. Lu, M. Nastasi, B. Cui, Influence of laser shock peening on irradiation defects in austenitic stainless steels, J. Nucl. Mater. 489 (2017) 203–210.
[95] Z. Shang, Jin Li, C. Fan, Y. Chen, Q. Li, H. Wang, T.D. Shen, X. Zhang, *In situ* study on surface roughening in radiation-resistant Ag nanowires, Nanotechnology 29 (2018).